THE JOURNAL OF PHYSICAL CHEMISTRY B

Article

pubs.acs.org/JPCB

^{15}N and ^{1}H Solid-State NMR Investigation of a Canonical Low-Barrier Hydrogen-Bond Compound: 1,8-Bis(dimethylamino)naphthalene

Paul B. White and Mei Hong*

Department of Chemistry, Massachusetts Institute of Technology, 170 Albany Street, Cambridge, Massachusetts 02139, United States

Supporting Information

ABSTRACT: Strong or low-barrier hydrogen bonds have often been proposed in proteins to explain enzyme catalysis and proton-transfer reactions. So far ^{1}H chemical shifts and scalar couplings have been used as the main NMR spectroscopic signatures for strong H-bonds. In this work, we report simultaneous measurements of ^{15}N and ^{1}H chemical shifts and N−H bond lengths by solid-state NMR in ^{15}N-labeled 1,8-bis(dimethylamino)naphthalene (DMAN), which contains a well-known strong NHN H-bond. We complexed DMAN with three different counteranions to examine the effects of the chemical environment on the H-bond lengths and chemical shifts. All three DMAN compounds exhibit significantly elongated N−H distances compared to the covalent bond length, and the $^{1}H^{N}$ chemical shifts are larger than ∼17 ppm, consistent with strong NHN H-bonds in the DMAN cation. However, the ^{15}N and ^{1}H chemical shifts and the precise N−H distances differ among the three compounds, and the ^{15}N chemical shifts show opposite dependences on the proton localization from the general trend in organic compounds, indicating the significant effects of the counteranions on the electronic structure of the H-bond. These data provide useful NMR benchmarks for strong H-bonds and caution against the sole reliance on chemical shifts for identifying strong H-bonds in proteins since neighboring side chains can exert influences on chemical shifts similar to those of the bulky organic anions in DMAN. Instead, N−H bond lengths should be measured, in conjunction with chemical shifts, as a more fundamental parameter of H-bond strength.

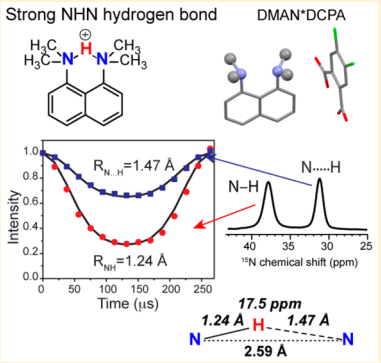

INTRODUCTION

Hydrogen bonding is ubiquitous in biological systems, and strong hydrogen bonds (H-bonds) have been proposed to play important roles in enzyme catalysis[1−5] and proton-transfer reactions in photoreceptors[6−9] and ion channels.[10,11] However, the nature and function of strong H-bonds have been the subject of significant debate in the literature. Early NMR spectroscopic studies of the catalytic triad of α-chymotrypsin reported an unusually large ^{1}H chemical shift of ∼18 ppm for the proton bound to Nδ1 of His57.[12] Combined with subsequent findings of low $^{1}H/^{2}H$ fractionation factors and large chemical shift perturbation, these data supported the existence of strong H-bonds in this and other enzymes.[13−15]

The fundamental criterion for classifying H-bond strengths is the potential energy curve (Scheme 1). Strong H-bonds are characterized by the fact that the ground vibrational mode for proton motion lies either near or above the energy barrier for proton transfer.[12,16,17] Two types of strong H-bonds are especially noteworthy: single-well H-bonds, which have no barrier for proton transfer, and low-barrier H-bonds (LBHB), which have a double-well energy minimum (Scheme 1e,f). In both of these strong H-bonds, the probability density function for proton position has a single maximum at the center of the two heteroatoms. A rigorous identification of the nature of H-bonds thus requires a study of the system's electronic and energetic states, which have been conducted largely with computational methods.[18−20]

Since potential energies of H-bonds are difficult to measure experimentally, distances have been used as alternative criteria for classifying H-bonds. For NHN compounds, these are the distance between the donor and acceptor nitrogens, R_{NN}, and the distances of the proton (H^{N}) from the donor (R_{NH}) and acceptor ($R_{N\cdots H}$). At one end of the hydrogen-bonding spectrum are weak or regular H-bonds (Scheme 1a), in which the ground vibrational energy is much lower than the proton-transfer barrier, and thus the probability density function for the proton has two maxima, centered near each heteroatom. Weak NHN H-bonds exhibit a much shorter R_{NH} than $R_{N\cdots H}$, an R_{NN} distance longer than 3.0 Å, and are primarily electrostatic in nature.[21,22] As the H-bonding strength increases, the H^{N} moves progressively toward the center of the two nitrogens, and R_{NN} decreases, making the bond more covalent than electrostatic. Strong NHN H-bonds (Scheme 1c,e,f) have $R_{NN} \leq 2.65$ Å. The degree of covalency of the H-bonds is manifested by the chemical shift of the intervening proton and the two-bond J-couplings between the nitrogens, $^{2h}J_{NN}$:[23−27] both the ^{1}H chemical shift and $^{2h}J_{NN}$ increase as the proton becomes more delocalized and the H-bond strength increases. For LBHBs (Scheme 1e), the shared proton between the donor

Received: June 27, 2015
Revised: August 5, 2015
Published: August 5, 2015

DOI: 10.1021/acs.jpcb.5b06171
J. Phys. Chem. B 2015, 119, 11581−11589

Scheme 1. Physical and Energy Properties of NHN Hydrogen Bonds and Proposed Potential-Energy Wells for the DMAN*HX Salts Studied Here

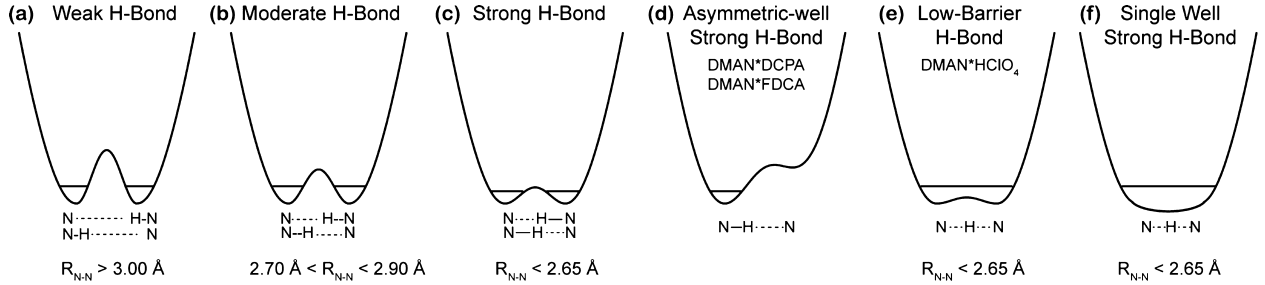

and acceptor is expected to have a chemical shift above ∼17 ppm.[28,29]

We became interested in better understanding H-bonds in biological systems through our studies of the influenza A M2 protein.[30] M2 forms a tetrameric proton channel in the virus envelope that is responsible for the acidification of the virion and the subsequent virus uncoating. The proton-selective residue in M2 is a single histidine, His37, in the transmembrane domain,[31] which contains both an H-bond donor (N−H) and acceptor (N:) in the imidazole ring. Several mechanisms of proton conduction have been proposed. In the shuttle model, the His37 imidazole alternately protonates and deprotonates by proton transfer with water molecules.[32] To generate the initial state for the next proton relay, the imidazole was thought to undergo ring flips and tautomerization, both of which have been observed experimentally.[33,34] The H-bonds in this shuttle model are weak NHO H-bonds between histidine and water. A high-resolution crystal structure reported tightly bound water molecules in the vicinity of the H37 tetrad,[35] and low-temperature imidazole H^N chemical shifts measured by NMR under conditions where proton transfer is frozen are less than 15 ppm, supporting weak to moderate H-bonds. Moreover, at high temperature when proton exchange is active, the imidazole H^N chemical shifts change to the water ^{1}H chemical shift value of ∼4.9 ppm, indicating that the H-bonding partner of the His37 side chain is water.[36] These lines of evidence support the weak water−histidine H-bonded shuttle mechanism. In comparison, an alternative proton-conduction model posits that a neutral imidazole ring of one polypeptide chain forms a strong or low-barrier H-bond with a cationic imidazolium of a neighboring chain at mildly acidic pH, prior to channel activation at lower pH.[10,11] This model was proposed to explain the observations that the first two pK_a's of the His37 tetrad are significantly elevated (8.2) compared to the typical pK_a of histidines in solution and moreover are unresolved,[10] suggesting that the M2 channel is able to store +2 charges before it becomes conductive. It is thought that a strong or low-barrier imidazole−imidazolium NHN H-bond can provide the mechanism for this charge stabilization. An implication of this LBHB model is that the tetramer consists of two structurally distinct units, or a dimer of dimers. Partial evidence for dimer formation was reported as doubled NMR chemical shifts for many residues in the protein;[37−39] however, this chemical shift doubling was observed at high pH where all histidines are neutral, thus violating the requirement of an imidazole−imidazolium pair in the LBHB model.

These studies of H-bonding in M2 and other complex biological systems inspired us to obtain better and clearer solid-state NMR (SSNMR) signatures of strong H-bonds, to correlate multiple signatures, and to delineate the environmental factors that may affect the H-bond strengths or their manifestations. So far few studies have correlated the readily measurable ^{1}H and ^{15}N chemical shifts with the less easily measured but more definitive parameter of R_{NH} distances. Given vibrational averaging effects and the low electron density of protons, N−H bond lengths obtained from X-ray crystallography are often imprecise and shorter than those measured by neutron diffraction and SSNMR. Thus, it is important to directly measure, in known strong H-bonds, R_{NH} distances by NMR and correlate them with ^{15}N and ^{1}H chemical shifts. In this article, we report a systematic study of these three NMR observables for the 1,8-bis(dimethylamino) naphthalene (DMAN) family of strong H-bond compounds. X-ray and neutron diffraction of DMAN salts showed R_{NN} distances of 2.55−2.63 Å.[22,40−43] For a small number of these compounds, R_{NH} and $R_{N\cdots H}$ distances have been reported by X-ray crystallography and have been found to range from equivalent (1.31 Å) to off-center. ^{1}H NMR chemical shifts of >18 ppm have been reported for DMAN salts containing small inorganic counterions,[28,43] but DMAN cations that are complexed with bulky organic anions, which better mimic protein side chains, are less studied. We have thus chosen several DMAN compounds with organic counteranions, synthesized them with ^{15}N and ^{13}C labeling, and measured N−H bond lengths and ^{15}N and ^{1}H chemical shifts. The results should provide useful NMR fingerprints of strong H-bonds in biological macromolecules.

EXPERIMENTAL SECTION

Synthesis of ^{15}N, ^{13}C-Labeled DMAN. DMAN was synthesized using modified literature procedures outlined in Scheme 2.[44−47] Naphthalene (783 mg, 6.12 mmol), $NH_4{}^{15}NO_3$ (1 g, 12.3 mmol, 2.01 equiv), and chloroform (6 mL) were added to a 50 mL round-bottomed flask, and the mixture was

Scheme 2. Synthesis Route to DMAN

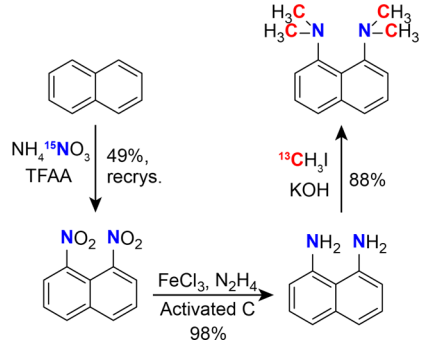

DOI: 10.1021/acs.jpcb.5b06171
J. Phys. Chem. B 2015, 119, 11581−11589

stirred. An addition funnel was added to the top of the flask, and the whole system was placed under N_2 gas. Trifluoroacetic anhydride (5 mL, 35.4 mmol, 5.8 equiv) was added to the addition funnel and introduced into the reaction flask via slow drip over 1.5 h. The solution became homogeneous and changed from colorless to rose to yellow during the addition. The reaction was stirred overnight under N_2. The resulting heterogeneous reaction mixture was then put on ice, and 10 mL of H_2O was slowly added to the flask by addition funnel to quench excess TFAA. The contents were poured into a separatory funnel containing 60 mL of H_2O and 20 mL of $CHCl_3$. The organic layer was extracted three more times with 20 mL of $CHCl_3$, and the combined organic fractions were dried over $MgSO_4$ and filtered before the solvent was removed on a rotary evaporator to yield an orange-yellow crude mixture consisting of a 3:1 mixture of $^{15}N_2$-1,8-dinitronaphthalene and $^{15}N_2$-1,5-dinitronaphthalene (1.25 g, 93%). The 1,8 isomer was purified first with a basic Al_2O_3 column and eluted with benzene (1,8 isomer, R_f = 0.4; 1,5 isomer, R_f = 0.76). The 1,8-rich fractions were collected and recrystallized three times with EtOAc. The supernatant of each crystallization was collected, and the solvent was removed under reduced pressure. The resulting solid was again recrystallized with EtOAc. The recrystallization process was repeated one more time to give a total of 608 mg (65% recovery, 49% overall yield) of $^{15}N_2$-1,8-dinitronaphthalene as yellow plates. ^{1}H NMR (400 MHz, $CDCl_3$): δ 7.75 (t, $^3J_{HH}$ = 7.9 Hz, 2H), 8.24 (d, $^3J_{HH}$ = 8.3 Hz, 2H), 8.30 (dd, $^3J_{HH}$ = 7.6 Hz, $^3J_{NH}$ = 2 Hz, 2H).

$^{15}N_2$-labeled 1,8-dinitronaphthalene (604 mg, 2.74 mmol), $FeCl_3$ hexahydrate (22 mg, 3 mol %), and Nuchar SA activated carbon (45 mg) were combined in a 25 mL round-bottomed flask equipped with a stir bar and a reflux condenser. MeOH (6 mL) and 50−60% N_2H_4 (464 μL, 5.45 equiv) were added, and the reaction was stirred and heated to 65 °C. After 5.5 h an aliquot was removed, and the reaction progress was checked by ^{1}H NMR. There was 7% remaining starting material, so 2 drops of hydrazine was added and stirred for another hour, after which no more starting material was observed. The reaction was cooled to room temperature and filtered over Celite, and the filter cake was washed with MeOH. The filtrate was removed under reduced pressure to yield a crude oil (430 mg, 98%), which was the pure $^{15}N_2$-1,8-diaminonaphthalene compound as verified by NMR. $^{15}N_2$-1,8-Diaminonaphthalene was used without purification for the next step. ^{1}H NMR (400 MHz, $CDCl_3$): δ 4.62 (bs, 4H, $^{15}NH_2$), 6.60 (d, $^3J_{HH}$ = 7 Hz, 2H), 7.15−7.22 (m, 4H).

$^{15}N_2$-1,8-Diaminonaphthalene (430 mg, 2.68 mmol) was added to a 10 mL round-bottomed flask equipped with a stir bar and placed under N_2 gas. Anhydrous DMSO (4 mL) was quickly added, the contents were stirred, and then KOH (775 mg, 5.15 equiv) was quickly added. The flask was placed in a room-temperature water bath, to which ^{13}CHI (950 μL, 5.6 equiv) was slowly added and stirred for 2.25 h. The temperature was then raised to 100 °C over 1 h, at which point KOH (320 mg, 2.1 equiv) was added. The reaction was stirred at 100 °C for another 40 min and then cooled to 50 °C. The reaction contents were quickly poured into a separatory funnel containing 150 mL of 2 M NaOH and 50 mL of Et_2O. The organic layer was washed with 3 × 50 mL of 2 M NaOH and then collected. The combined aqueous layers were extracted with 2 × 50 mL of Et_2O. The combined organic layers were dried with $MgSO_4$ and filtered, and the solvent was removed under reduced pressure, resulting in a red oil (532 mg, 2.42 mmol, 90%) that crystallized into needles upon refrigeration and was pure by ^{1}H NMR. δ 2.83 (dd, $^1J_{CH}$ = 138.7 Hz, $^2J_{NH}$ = 4.1 Hz, 12H), 6.96 (broad d, $^3J_{HH}$ = 7.4 Hz, 2H), 7.33 (t, $^3J_{HH}$ = 7.6 Hz, 2H), 7.38 (d, $^3J_{HH}$ = 7.7 Hz, 2H).

The ^{15}N,^{13}C-labeled $DMANH^+$ salts were recrystallized with three counterions: perchlorate ($HClO_4$), 4,5-dichlorophthalic acid (DCPA), and furan-3,4-dicarboxylic acid (FDCA). DMAN*$HClO_4$ was formed by dissolving DMAN in diethyl ether, stirring the solution, and adding concentrated $HClO_4$(aq) dropwise. DMAN*$HClO_4$ precipitated as a brown material, and the addition of $HClO_4$ ceased when no more precipitate formed. The stirring was then stopped, the supernatant pipetted out, and the precipitate washed three times with diethyl ether and then dried under vacuum. The resulting goo was recrystallized twice from a minimal amount of boiling acetonitrile. DMAN*DCPA and DMAN*FDCA were formed by adding DMAN and the respective acid as solids to a 1.5 mL HPLC vial, dissolving them in a minimal amount of hot acetonitrile and then letting the solution cool. Afterward, the DMAN*DCPA and DMAN*FDCA solutions were allowed to evaporate slowly at room temperature. The resulting crystals were recrystallized once more, washed with a very small amount of cold acetonitrile, and dried. The structures of DMAN*$HClO_4$ and DMAN*FDCA were solved using X-ray diffraction since no structure existed for DMAN*$HClO_4$ and, despite multiple attempts, the exact unit cell obtained by Wozniak for DMAN*FDCA could not be reproduced.[42] Instead, a unique unit cell with the same molecular composition (DMAN + FDCA + water) was obtained. The unit cell of DMAN*DCPA matched the literature unit cell, and no further X-ray analysis was performed.

Solid-State NMR Spectroscopy. All experiments were conducted using Bruker 400 and 600 MHz solid-state NMR spectrometers equipped with 4 mm or 3.2 mm magic-angle-spinning (MAS) probes. Typical radiofrequency (rf) field strengths were 40−50 kHz for ^{15}N and 80−100 kHz for ^{1}H. The experiments were conducted at both ambient temperature and 95 K to investigate the degree of proton dynamics at ambient temperature. ^{15}N cross-polarization (CP) spectra were measured under an MAS frequency of 7.58 kHz, while ^{1}H spectra were measured under 15 kHz MAS. ^{15}N chemical shifts were externally referenced to the *N*-acetyl-valine ^{15}N chemical shift of 122.0 ppm on the liquid ammonium scale. ^{1}H chemical shifts were referenced to the published values of the tripeptide formyl-MLF-OH.[48] N−H bond lengths were measured using the dipolar-doubled 2D ^{15}N−^{1}H dipolar chemical shift (DIPSHIFT) correlation experiment[49] under 3.79 kHz MAS. ^{1}H homonuclear decoupling was conducted using the FSLG sequence,[50] which has a theoretical scaling factor of 0.577. The experimental scaling factor was measured using formyl-MLF−OH[51,52] and was found to be 0.577 at ambient temperature and 0.610 at 95 K. Two-dimensional ^{15}N−^{1}H HETCOR spectra were measured under 7.58 kHz MAS. Lee−Goldburg (LG) CP[53,54] with a 1 ms contact time and a 50 kHz effective spin-lock field was used to transfer the ^{1}H polarization to ^{15}N without ^{1}H spin diffusion. ^{1}H homonuclear decoupling during the t_1 evolution period was carried out using the FSLG sequence with a transverse field strength of 80 kHz.

RESULTS

X-ray Diffraction Data of Selected DMAN Compounds. We chose three compounds from the many known DMAN salts using two criteria.[40,42,55−57] First, each recrystal-

DOI: 10.1021/acs.jpcb.5b06171
J. Phys. Chem. B 2015, 119, 11581−11589

lization should give a single-crystalline form since the bulk separation of polymorphic crystals is often incomplete, which would complicate spectral interpretation. Second, DMAN salts with a highly delocalized proton as well as more localized protons are needed to compare the chemical shifts and bond lengths for different strengths of H-bonds. On the basis of the literature, we chose DMAN*DCPA and DMAN*FDCA as examples of salts with bulky organic counteranions (Figure 1)[42] that contain partially localized H^N protons and DMAN*$HClO_4$ as a potential model system with a delocalized H^N.

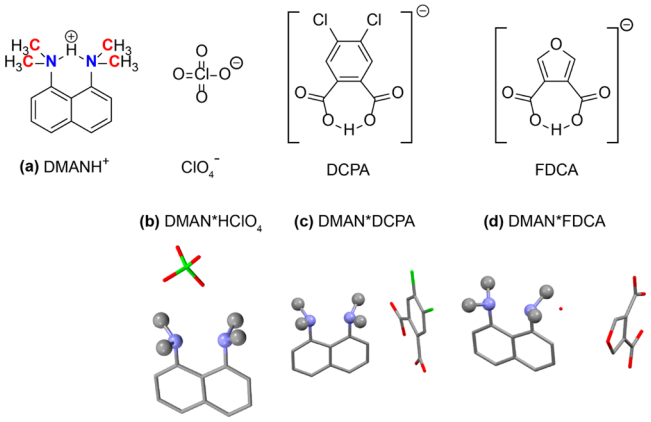

Figure 1. Structures of the DMAN salts used in this study. (a) Chemical structures. (b–d) X-ray crystal structures. (b) DMAN*$HClO_4$. (c) DMAN*DCPA. (d) DMAN*FDCA. Hydrogen atoms are omitted for clarity. The structure for DMAN*DCPA is reproduced from ref 42.

We first verified the structures of the recrystallized DMAN salts by X-ray diffraction (Figure 1). DMAN*$HClO_4$ has not been previously characterized by X-ray diffraction, thus a full atomic structure was determined. The unit cell for DMAN*DCPA matched the literature result while the unit cell of DMAN*FDCA differed significantly from the literature[42] (Table 1). Upon obtaining a full data set, we found that the

Table 1. Unit Cell Parameters of the Crystal Structures of the Three DMAN Salts Used in This Study

	DMAN*HClO4	DMAN*DCPA	DMAN*FDCA
crystal group	*Fdd*2	*P*1	*P*21/*n*
α (deg)	90.00	75.13	90.00
β (deg)	90.00	71.23	91.65
γ (deg)	90.00	70.62	90.00
a (Å)	12.55	9.30	11.24
b (Å)	46.88	9.63	10.28
c (Å)	10.24	13.03	16.69
volume (Å^3)	6022.69	1027.63	1928.04

FDCA in our crystal has a different spatial arrangement with respect to the DMAN cation. In addition, there is 1 equiv of water in the DMAN*FDCA unit cell, which is absent in the other two salts, but the water molecule has a different position in our crystal from that of the literature.

Comparison of the three DMAN crystal structures reveals small but important differences. First, despite the common cation, the R_{NN} distance differs among the three compounds. The distance is the shortest for DMAN*$HClO_4$ (2.55 Å) and increases to 2.59 Å for DMAN*DCPA and 2.62 Å for DMAN*FDCA. Second, the inorganic perchlorate anion rests proximally above the NHN H-bond, roughly equidistant to the two dimethylamino groups, whereas the organic DCPA and FDCA anions lie on one side of the NHN H-bond. The nearest heavy-atom distance between the nitrogen donor/acceptors and the counteranion is 3.30 Å for DMAN*$HClO_4$, 3.85 Å for DMAN*DCPA, and 3.64 Å for DMAN*FDCA. The proximity and orientation of the anion to the NHN H-bond and the differences in R_{NN} may affect the localization of the proton by changing the chemical environment at the nitrogen donors and acceptors.

^{15}N Chemical Shifts and N–H Distances in DMAN Salts. Figure 2 shows the ^{15}N CP-MAS spectra of the three

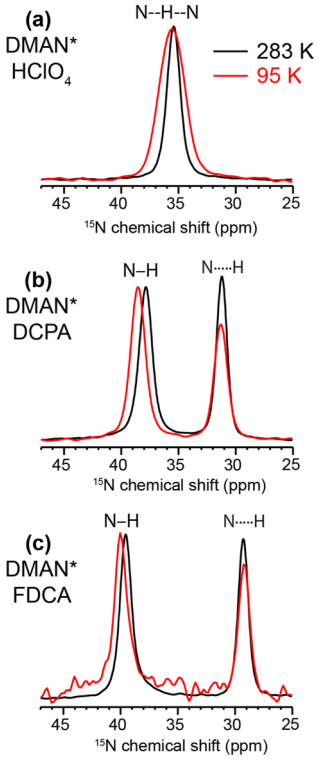

Figure 2. ^{15}N CPMAS spectra of DMAN salts at 283 and 95 K. (a) DMAN*$HClO_4$. (b) DMAN*DCPA. (c) DMAN*FDCA. The N–H and N···H assignments are based on the DIPSHIFT data in Figure 3.

DMAN compounds at 283 and 95 K. Consistent with the crystal structure, the compound with the shortest R_{NN} distance and the highest unit cell symmetry, DMAN*$HClO_4$, exhibits a single ^{15}N peak at 35.4 ppm. In comparison, DMAN*DCPA and DMAN*FDCA display two ^{15}N chemical shifts, 37.8 and 31.2 ppm for the DCPA salt and 39.5 and 29.3 ppm for the FDCA salt, suggesting that the proton is located asymmetrically between the two nitrogens. DMAN*DCPA has a smaller ^{15}N chemical shift difference (6.6 ppm) than DMAN*FDCA (10.2 ppm), but the average of the two ^{15}N chemical shifts, 34.4 ppm, is close to the single ^{15}N chemical shift of DMAN*$HClO_4$.

In general, ^{15}N chemical shifts of organic compounds follow the trend that larger (downfield) shifts correspond to more deprotonated nitrogens with longer R_{NH} bond lengths, while smaller (upfield) chemical shifts indicate more protonated nitrogens with shorter R_{NH} bond lengths. Interestingly, direct measurement of the N–H distance in the three DMAN compounds shows deviations from this rule. We used the dipolar-doubled DIPSHIFT experiment to measure the

DOI: 10.1021/acs.jpcb.5b06171
J. Phys. Chem. B 2015, 119, 11581–11589

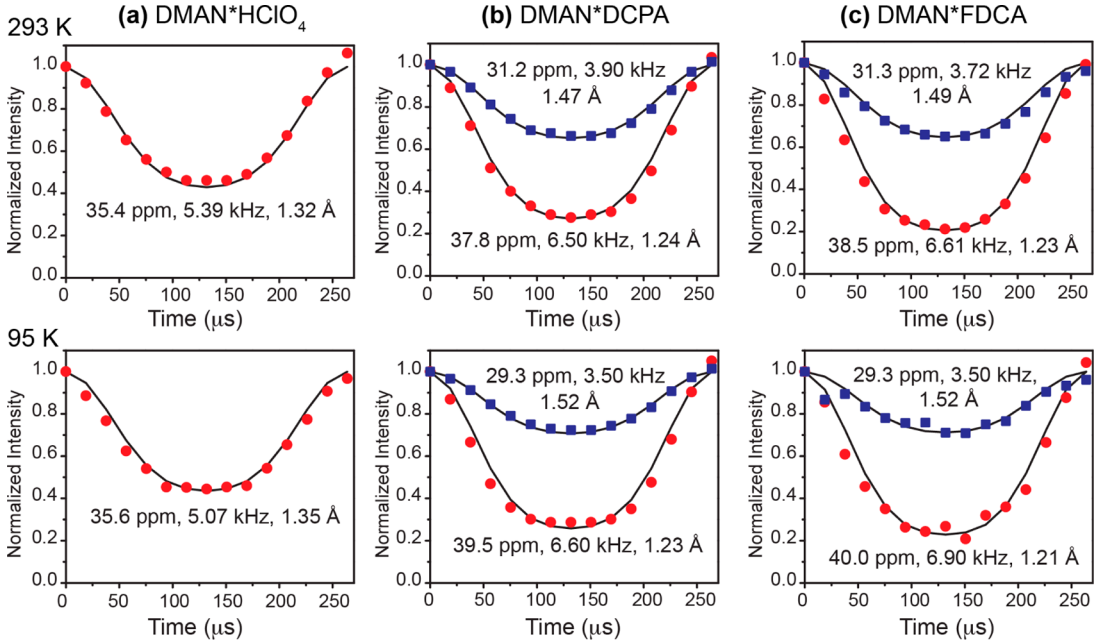

Figure 3. $^{15}N-^{1}H$ doubled-DIPSHIFT data of DMAN salts at 293 K (top) and 95 K (bottom). (a) DMAN*$HClO_4$. (b) DMAN*DCPA. (c) DMAN*FDCA. The data were obtained under 3.79 kHz MAS. Solid lines are best-fit simulations. The listed N−H dipolar coupling strengths are true values after taking into account the experimental FSLG scaling factor and the doubling factor. The ^{15}N chemical shift and the N−H distances are also indicated.

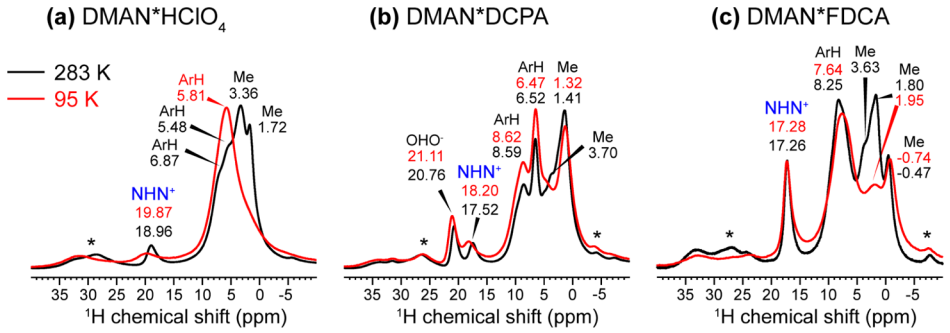

Figure 4. ^{1}H MAS spectra of DMAN salts at 283 K (black) and 95 K (red) under 15 kHz MAS. Assignment is based on the general chemical shift trends of aromatic, H^N, and aliphatic protons. Asterisks indicate spinning sidebands.

$^{15}N-^{1}H$ dipolar coupling and R_{NH} distances (Figure 3). Motion in these rigid organic crystals is negligible, thus the measured coupling constant directly indicates the internuclear distance. At ambient temperature, the single ^{15}N peak of the perchlorate compound exhibits a $^{15}N-^{1}H$ dipolar coupling of 5.39 kHz, which translates to an R_{NH} of 1.32 Å. This distance is in good agreement with the R_{NH} of 1.31 Å in the crystal structure of DMAN salts that contain an equally shared proton, such as DMAN*HBr[56] and DMAN*tetrazole.[40] In DMAN*DCPA, the downfield peak has a 6.50 kHz coupling, corresponding to an R_{NH} of 1.24 Å, while the upfield ^{15}N peak has a longer R_{NH} of 1.47 Å. For DMAN*FDCA, the downfield ^{15}N peak has an R_{NH} distance of 1.23 Å while the upfield ^{15}N peak has an R_{NH} of 1.49 Å. Thus, for the DCPA and FDCA salts, the more deshielded (or downfield) ^{15}N resonance has a stronger $^{15}N-^{1}H$ dipolar coupling or a shorter R_{NH} bond length than the upfield ^{15}N peak, opposite from the general trend, suggesting that the two nitrogens' spectroscopic signatures are significantly perturbed by the counteranions.

We repeated the ^{15}N CP-MAS and N−H DIPSHIFT experiments at 95 K to determine if there is noticeable proton dynamics at ambient temperature and if the H^N proton becomes more localized to one of the two nitrogens at low temperature. The ^{15}N chemical shift showed negligible changes with temperature, but the line width broadened significantly for DMAN*$HClO_4$, from 55 Hz at ambient temperature to 109 Hz at 95 K. In comparison, the DMAN*DCPA and DMAN*FDCA ^{15}N peaks show only minor line broadening of ∼10 Hz. The $^{15}N-^{1}H$ dipolar couplings remain unchanged within experimental uncertainty from 293 to 95 K, indicating that the H^N position is insensitive to temperature in this range.

$^{1}H^N$ Chemical Shifts of DMAN Salts. We next measured the acidic proton's chemical shift to correlate with the ^{15}N chemical shift and R_{NH} bond lengths. The chemical shift differences between the H^N and aliphatic protons are sufficiently large that 1D ^{1}H MAS spectra are already effective in resolving them (Figure 4). At 600 MHz under 15 kHz MAS, the 1D ^{1}H spectra show sufficient resolution at both 283 and 95 K. For DMAN*$HClO_4$, the NHN^+ proton resonates at 18.9 ppm while the methyl protons resonate at 3.50 and 1.70 ppm, in good agreement with literature values.[43] In addition, two

DOI: 10.1021/acs.jpcb.5b06171
J. Phys. Chem. B 2015, 119, 11581−11589

resonances at 6.87 and 5.48 ppm were observed and assigned to aromatic protons.

The ^{1}H spectrum of DMAN*DCPA shows more resolved peaks. Two large ^{1}H chemical shifts at 20.76 and 17.52 ppm are detected and likely correspond to the OHO$^-$ proton of the DCPA anion and the NHN$^+$ proton of the DMAN cation, respectively. The 8.59 and 6.52 ppm peaks can be assigned to the naphthalene ring protons, while the 3.70 and 1.41 ppm peaks are assigned to the *N*-methyl groups. DMAN*FDCA exhibited a single downfield ^{1}H peak at 17.26 ppm, despite having a similar OHO$^-$ proton as in DMAN*DCPA. We attribute this to coincidental overlap of the NHN$^+$ and OHO$^-$ chemical shifts, which is consistent with the high intensity of this peak compared to the aromatic and aliphatic signals. Similar to DMAN*DCPA, the aromatic ^{1}H resonances are well resolved at 8.25 ppm and the methyl ^{1}H signals span from 3.63 to −0.47 ppm. The −0.47 ppm resonance likely results from the methyl group that is flanked by the π-cloud of the FDCA anion and the naphthalene ring of a neighboring DMANH$^+$ cation in the crystal lattice, which causes additional shielding from the aromatic electrons.

For DMAN*DCPA, the 1D ^{1}H MAS spectrum alone cannot unambiguously determine which of the two downfield signals belongs to the NHN$^+$ H-bond. Thus, we recorded 2D ^{15}N−^{1}H HETCOR spectra to make a definitive assignment. Figure 5

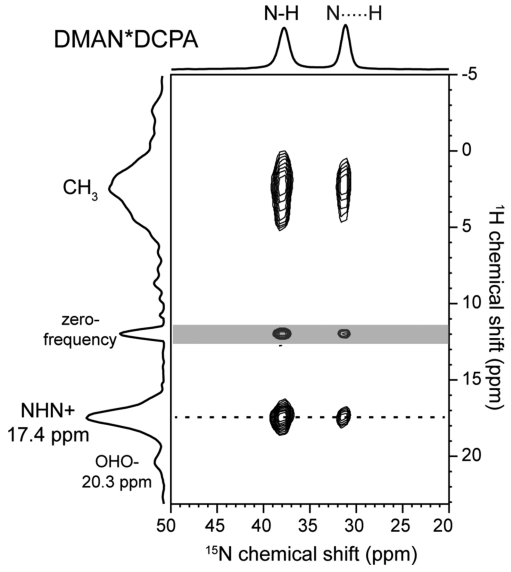

Figure 5. Two-dimensional ^{15}N−^{1}H HETCOR spectrum of DMAN*DCPA at 293 K under 7.58 kHz MAS. The ^{1}H chemical shift is the true value after taking into account the FLSG scaling factor of 0.577.

shows two ^{1}H−^{15}N cross peaks at (17.4 ppm, 37.8 ppm) and (17.4 ppm, 31.2 ppm), thus confirming the assignment of the NHN$^+$ proton to 17.4 ppm. The OHO$^-$ proton then resonates at 20.76 ppm, consistent with the fact that it lies in a very short and strong H-bond. The 2D HETCOR spectra of the other two DMAN compounds (not shown) also confirmed the ^{1}H chemical shift assignment in the 1D ^{1}H spectra.

DISCUSSION

While hydrogen bonding has undisputed importance in biological and synthetic compounds, rigorous studies of the NMR signatures of hydrogen bonding in the solid state are relatively scarce. McDermott and co-workers investigated NHN H-bonds in imidazole−imidazolium complexes with different counterions by measuring temperature-dependent ^{15}N chemical shifts and correlating these with crystallographically determined R_{NN} distances.[58] The R_{NN} values were 2.65−2.68 Å, which are slightly longer than the cutoff for strong H-bonds. Their NMR data revealed the presence of fast proton exchange in some of the salts from 200 to 280 K, and the population of the two protonation states is strongly dependent on temperature and counteranions. At 210 K, these workers measured an R_{NH} distance of 1.10 Å, which is close to the covalent bond length of R_{NH} = 1.05 Å in imidazole.[22] The temperature-dependent ^{15}N chemical shifts, nearly covalent R_{NH} bond lengths, and modest R_{NN} distances together indicate that the imidazole−imidazolium complexes contain weak to moderate H-bonds.

The intramolecular strong H-bonds formed by DMAN differ qualitatively from the intermolecular weak H-bonds in imidazoles. Figure 6 summarizes the measured chemical shifts

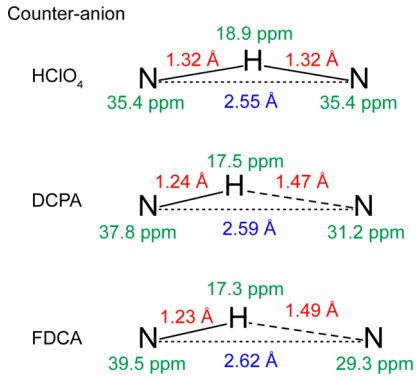

Figure 6. Summary of the ^{1}H and ^{15}N NMR chemical shifts (green), N−H bond lengths (red), and crystallographically determined N···N distances (blue) of the three DMAN salts. DMAN*HClO$_4$ shows the most delocalized H^N or the strongest H-bond, the largest ^{1}H chemical shift, and equivalent ^{15}N chemical shifts. The two DMAN salts with bulky organic counteranions have different R_{NH} values, inequivalent ^{15}N chemical shifts, and smaller ^{1}H chemical shifts.

and R_{NH} distances in our DMAN compounds. All three compounds show ^{1}H^N chemical shifts larger than ∼17 ppm, which is generally accepted as the lower limit for strong H-bonds.[27−29] Despite this large ^{1}H chemical shift, the nitrogens in DMAN*DCPA and DMAN*FDCA are not chemically equivalent, as seen by two resolved ^{15}N chemical shifts (Figure 2). This is caused by the fact that the bulky organic DCPA and FDCA anions are positioned asymmetrically with respect to the DMANH$^+$ cation, creating different chemical environments for the two nitrogens. In comparison, smaller counteranions, such as mineral acids, perchlorate, and tetrafluoroborate, do not exert as large an effect on the ^{15}N chemical environment, as seen from the X-ray and ^{15}N NMR studies of Limbach and co-workers.[41]

The distinct nitrogen environments affect the basicity of the nitrogen lone-pair electron and in turn the proton localization.[27] Both DMAN*DCPA and DMAN*FDCA show a partially localized proton based on the measured R_{NH} distances, and this proton localization correlates with a decrease in the ^{1}H chemical shift (Figure 6). This correlation is understandable since a more covalently bonded proton is more shielded by the heteroatom's electrons. Similar correlations between ^{1}H chemical shifts and R_{NH} have been observed for DMAN salts

DOI: 10.1021/acs.jpcb.5b06171
J. Phys. Chem. B 2015, 119, 11581−11589

formed from mineral acids and organic acids.[43] The mineral acids caused more equally shared H^N protons and the resulting H^N chemical shifts ranged from 20.7 to 18.8 ppm, whereas the organic acids caused more localized protons and the ^1H chemical shifts ranged from 18.6 to 16.9 ppm. The large effects of the counteranion on the charge density profiles of the DMAN cation have been previously observed in DMAN salts such as DMAN*picrate[41] and DMAN*PF_6,[42,43,55,59,60] and even minor polarization differences in the nitrogen lone pair have been shown to cause modest to large changes in R_{NH} and $R_{N\cdots H}$.

While the two R_{NH} distances in DMAN*DCPA and DMAN*FDCA are not equivalent, both distances are much longer than the covalent bond length of 1.1 Å, and both compounds also have relatively short R_{NN} distances. These results indicate that DMAN complexed with DCPA and FDCA contains a strong NHN^+ H-bond with an asymmetric double-well potential (Scheme 1d). In comparison, the NHN^+ H-bond in DMAN*$HClO_4$ has a symmetric double-well potential with a low barrier (Scheme 1e) because a single ^{15}N peak and a single $^1H^N$ peak were observed at both high and low temperatures. Proton motion in this LBHB is instantaneous but over a very small distance, thus making the two R_{NH} distances indistinguishable. That the DMAN*$HClO_4$ potential energy curve still has a barrier rather than being barrierless (Scheme 1f) is manifested by the fact that the ^{15}N and ^1H peaks are both broadened at low temperature, while a barrierless single-well potential should exhibit no temperature-dependent line widths or chemical shifts.

In conclusion, the proton position along the H-bond and the strength of the H-bond in DMAN compounds are extremely sensitive to the distant effects of the anion. This sensitivity calls into question the likelihood of establishing and preserving strong H-bonds in complex macromolecules such as proteins. While strong- and low-barrier H-bonds have been proposed in proteins such as chymotrypsin, ketosteroid isomerases, and M2, the necessary distances are rarely measured. Instead, a large downfield ^1H chemical shift is often used as proof of strong H-bonds. However, a large ^1H chemical shift is not definitive proof of a strong H-bond since side chains and charged residues in close proximity to the H-bond of interest can exert significant influence on the ^1H chemical shift. For example, the π-bond node of aromatic side chains and electrostatic interactions between a downfield proton such as in carboxylic acids (around 12−14 ppm) and another group can cause large downfield ^1H chemical shifts. On the other hand, small ^1H chemical shifts can rule out the existence of strong H-bonds. In other words, large ^1H chemical shifts are a necessary but not sufficient condition for strong or low-barrier H-bonds. For a strong H-bond to exist, the donor−acceptor distance must be significantly shorter than the sum of the van der Waals radii while the proton distance to the two heteroatoms must be significantly longer than the covalent bond length. While the heavy-atom distances can be readily measured by crystallography, the N−H or O−H distance cannot, thus NMR spectroscopy is an important tool for identifying strong H-bonds. In a true low-barrier H-bond, the proton in the H-bond should be equidistant between the donor and acceptor; in other words, the pK_a values of the donor and acceptor heteroatoms should be matched. Finally, as well documented in the literature, if the protein of interest functions in solution, then water further reduces the likelihood of LBHBs compared to the solid state because water oxygen can compete with the heteroatoms while water hydrogen can compete for the lone pairs in the LBHB.[61] For example, Yamaguchi recently reported crystallographic evidence for a LBHB between *para*-coumaric acid and Glu46 in the photoactive yellow protein, but in solution a small ^1H chemical shift of 15.2 ppm was found for the OHO^- proton and computational modeling further supported a regular H-bond.[5,8,9] Thus, transient interactions between water and biomolecules substantially decrease the likelihood of LBHBs in solution. These considerations argue against the presence of LBHBs between the proton-selective histidines in the water-filled pore of the influenza M2 channel, in addition to the experimental evidence of imidazole H^N chemical shifts near the water frequency and the X-ray crystal structure of a water cluster at the histidine tetrad.

■ ASSOCIATED CONTENT

Supporting Information

The Supporting Information is available free of charge on the ACS Publications website at DOI: 10.1021/acs.jpcb.5b06171.

Full author list for ref 35 (PDF)

■ AUTHOR INFORMATION

Corresponding Author

*E-mail: meihong@mit.edu.

Notes

The authors declare no competing financial interest.

■ ACKNOWLEDGMENTS

This work is supported by NIH grant GM088204 to M.H. We thank Dr. Marc Caporini and Dr. Melanie Rosay at Bruker Biospin for making the 400 and 600 MHz NMR spectrometers available for experiments at 95 K. We also thank Keith Fritzsching for insightful discussions on LBHBs and for initial exploratory experiments.

■ REFERENCES

(1) Cleland, W. W.; Frey, P. A.; Gerlt, J. A. The Low Barrier Hydrogen Bond in Enzymatic Catalysis. *J. Biol. Chem.* **1998**, *273*, 25529−25532.

(2) Langkilde, A.; Kristensen, S. M.; Lo Leggio, L.; Molgaard, A.; Jensen, J. H.; Houk, A. R.; Poulsen, J. C. N.; Kauppinen, S.; Larsen, S. Short Strong Hydrogen Bonds in Proteins: a Case Study of Rhamnogalacturonan Acetylesterase. *Acta Crystallogr., Sect. D: Biol. Crystallogr.* **2008**, *64*, 851−863.

(3) Polgar, L. The Catalytic Triad of Serine Peptidases. *Cell. Mol. Life Sci.* **2005**, *62*, 2161−2172.

(4) Pollack, R. M. Enzymatic Mechanisms for Catalysis of Enolization: Ketosteroid Isomerase. *Bioorg. Chem.* **2004**, *32*, 341−353.

(5) Sigala, P. A.; Tsuchida, M. A.; Herschlag, D. Hydrogen Bond Dynamics in the Active Site of Photoactive Yellow Protein. *Proc. Natl. Acad. Sci. U. S. A.* **2009**, *106*, 9232−9237.

(6) Bondar, A. N.; Fischer, S.; Smith, J. C. Water Pathways in the Bacteriorhodopsin Proton Pump. *J. Membr. Biol.* **2011**, *239*, 73−84.

(7) Mak-Jurkauskas, M. L.; Bajaj, V. S.; Hornstein, M. K.; Belenky, M.; Griffin, R. G.; Herzfeld, J. Energy Transformations Early in the Bacteriorhodopsin Photocycle Revealed by DNP-Enhanced Solid-State NMR. *Proc. Natl. Acad. Sci. U. S. A.* **2008**, *105*, 883−888.

(8) Nadal-Ferret, M.; Gelabert, R.; Moreno, M.; Lluch, J. M. Are There Really Low-Barrier Hydrogen Bonds in Proteins? The Case of Photoactive Yellow Protein. *J. Am. Chem. Soc.* **2014**, *136*, 3542−3552.

(9) Yamaguchi, S.; Kamikubo, H.; Kurihara, K.; Kuroki, R.; Niimura, N.; Shimizu, N.; Yamazaki, Y.; Kataoka, M. Low-Barrier Hydrogen Bond in Photoactive Yellow Protein. *Proc. Natl. Acad. Sci. U. S. A.* **2009**, *106*, 440−444.

DOI: 10.1021/acs.jpcb.5b06171
J. Phys. Chem. B 2015, 119, 11581−11589

(10) Hu, J.; Fu, R.; Nishimura, K.; Zhang, L.; Zhou, H. X.; Busath, D. D.; Vijayvergiya, V.; Cross, T. A. Histidines, Heart of the Hydrogen Ion Channel from Influenza A Virus: Toward an Understanding of Conductance and Proton Selectivity. *Proc. Natl. Acad. Sci. U. S. A.* **2006**, *103*, 6865−6870.
(11) Sharma, M.; Yi, M. G.; Dong, H.; Qin, H. J.; Peterson, E.; Busath, D. D.; Zhou, H. X.; Cross, T. A. Insight Into the Mechanism of the Influenza A Proton Channel from a Structure in a Lipid Bilayer. *Science* **2010**, *330*, 509−512.
(12) Frey, P. A.; Whitt, S. A.; Tobin, J. B. A Low-Barrier Hydrogen-Bond in the Catalytic Triad of Serine Proteases. *Science* **1994**, *264*, 1927−1930.
(13) Lin, J.; Westler, W. M.; Cleland, W. W.; Markley, J. L.; Frey, P. A. Fractionation Factors and Activation Energies for Exchange of the Low Barrier Hydrogen Bonding Proton in Peptidyl Trifluoromethyl Ketone Complexes of Chymotrypsin. *Proc. Natl. Acad. Sci. U. S. A.* **1998**, *95*, 14664−14668.
(14) Loh, S. N.; Markley, J. L. Hydrogen-Bonding in Proteins as Studied by Amide Hydrogen D/H-Fractionation Factors - Application to Staphylococcal Nuclease. *Biochemistry* **1994**, *33*, 1029−1036.
(15) Markley, J. L.; Westler, W. M. Protonation-State Dependence of Hydrogen Bond Strengths and Exchange Rates in a Serine Protease Catalytic Triad: Bovine Chymotrypsinogen A. *Biochemistry* **1996**, *35*, 11092−11097.
(16) GarciaViloca, M.; Gelabert, R.; GonzalezLafont, A.; Moreno, M.; Lluch, J. M. Is an Extremely Low-Field Proton Signal in the NMR Spectrum Conclusive Evidence for a Low-Barrier Hydrogen Bond? *J. Phys. Chem. A* **1997**, *101*, 8727−8733.
(17) Garcia-Viloca, M.; Gelabert, R.; Gonzalez-Lafont, A.; Moreno, M.; Lluch, J. M. Temperature Dependence of Proton NMR Chemical Shift as a Criterion to Identify Low-Barrier Hydrogen Bonds. *J. Am. Chem. Soc.* **1998**, *120*, 10203−10209.
(18) Schutz, C. N.; Warshel, A. The Low Barrier Hydrogen Bond (LBHB) Proposal Revisited: The Case of the Asp···His Pair in Serine Proteases. *Proteins: Struct., Funct., Genet.* **2004**, *55*, 711−723.
(19) Warshel, A.; Papazyan, A. Energy Considerations Show That Low-Barrier Hydrogen Bonds Do Not Offer a Catalytic Advantage Over Ordinary Hydrogen Bonds. *Proc. Natl. Acad. Sci. U. S. A.* **1996**, *93*, 13665−13670.
(20) Warshel, A.; Papazyan, A.; Kollman, P. A. On Low-Barrier Hydrogen-Bonds and Enzyme Catalysis. *Science* **1995**, *269*, 102−104.
(21) Emsley, J. Very Strong Hydrogen-Bonding. *Chem. Soc. Rev.* **1980**, *9*, 91−124.
(22) Malarski, Z.; Sobczyk, L.; Grech, E. Structure and IR Spectroscopic Behavior of NHN Hydrogen-Bonds. *J. Mol. Struct.* **1988**, *177*, 339−349.
(23) Benedict, H.; Shenderovich, I. G.; Malkina, O. L.; Malkin, V. G.; Denisov, G. S.; Golubev, N. S.; Limbach, H. H. Nuclear Scalar Spin-Spin Couplings and Geometries of Hydrogen Bonds. *J. Am. Chem. Soc.* **2000**, *122*, 1979−1988.
(24) Brown, S. P.; Perez-Torralba, M.; Sanz, D.; Claramunt, R. M.; Emsley, L. The Direct Detection of a Hydrogen Bond in the Solid State by NMR Through the Observation of a Hydrogen-Bond Mediated N-15-N-15 J Coupling. *J. Am. Chem. Soc.* **2002**, *124*, 1152−1153.
(25) Dingley, A. J.; Masse, J. E.; Peterson, R. D.; Barfield, M.; Feigon, J.; Grzesiek, S. Internucleotide Scalar Couplings Across Hydrogen Bonds in Watson-Crick and Hoogsteen Base Pairs of a DNA Triplex. *J. Am. Chem. Soc.* **1999**, *121*, 6019−6027.
(26) Pietrzak, M.; Limbach, H. H.; Perez-Torralba, M.; Sanz, D.; Claramunt, R. M.; Elguero, J. Scalar Coupling Constants Across the Intramolecular NHN Hydrogen Bond of Symmetrically and Non-Symmetrically Substituted 6-Aminofulvene-1-aldimines. *Magn. Reson. Chem.* **2001**, *39*, S100−S108.
(27) Pietrzak, M.; et al. Symmetrization of Cationic Hydrogen Bridges of Protonated Sponges Induced by Solvent and Counteranion Interactions as Revealed by NMR Spectroscopy. *Chem. - Eur. J.* **2010**, *16*, 1679−1690.
(28) Brycki, B.; Brzezinski, B.; Grech, E.; Malarski, Z.; Sobczyk, L. H-1 and C-13 NMR-Studies of 1,8-Bis(Dimethylamino)Naphthalene Salts in Acetonitrile-D3. *Magn. Reson. Chem.* **1991**, *29*, 558−560.
(29) Tobin, J. B.; Whitt, S. A.; Cassidy, C. S.; Frey, P. A. Low-Barrier Hydrogen-Bonding in Molecular-Complexes Analogous to Histidine and Aspartate in the Catalytic Triad of Serine Proteases. *Biochemistry* **1995**, *34*, 6919−6924.
(30) Hong, M.; DeGrado, W. F. Structural Basis for Proton Conduction and Inhibition by the Influenza M2 Protein. *Protein Sci.* **2012**, *21*, 1620−1633.
(31) Wang, C.; Lamb, R. A.; Pinto, L. H. Activation of the M2 Ion Channel of Influenza Virus: A Role for the Transmembrane Domain Histidine Residue. *Biophys. J.* **1995**, *69*, 1363−1371.
(32) Pinto, L. H.; Dieckmann, G. R.; Gandhi, C. S.; Papworth, C. G.; Braman, J.; Shaughnessy, M. A.; Lear, J. D.; Lamb, R. A.; DeGrado, W. F. A Functionally Defined Model for the M2 Proton Channel of Influenza A Virus Suggests a Mechanism for Its Ion Selectivity. *Proc. Natl. Acad. Sci. U. S. A.* **1997**, *94*, 11301−11306.
(33) Hu, F.; Luo, W.; Hong, M. Mechanisms of Proton Conduction and Gating by Influenza M2 Proton Channels from Solid-State NMR. *Science* **2010**, *330*, 505−508.
(34) Hu, F. H.; Schmidt-Rohr, K.; Hong, M. NMR Detection of pH-Dependent Histidine-Water Proton Exchange Reveals the Conduction Mechanism of a Transmembrane Proton Channel. *J. Am. Chem. Soc.* **2012**, *134*, 3703−3713.
(35) Acharya, A.; et al. Structural Mechanism of Proton Transport Through the Influenza A M2 Protein. *Proc. Natl. Acad. Sci. U. S. A.* **2010**, *107*, 15075−15080.
(36) Hong, M.; Fritzsching, K. J.; Williams, J. K. Hydrogen-Bonding Partner of the Proton-Conducting Histidine in the Influenza M2 Proton Channel Revealed From H-1 Chemical Shifts. *J. Am. Chem. Soc.* **2012**, *134*, 14753−14755.
(37) Andreas, L. B.; Eddy, M. T.; Pielak, R. M.; Chou, J. J.; Griffin, R. G. Magic Angle Spinning NMR Investigation of Influenza A M2(18−60): Support for an Allosteric Mechanism of Inhibition. *J. Am. Chem. Soc.* **2010**, *132*, 10958−10960.
(38) Andreas, L. B.; Eddy, M. T.; Chou, J. J.; Griffin, R. G. Magic-Angle-Spinning NMR of the Drug Resistant S31N M2 Proton Transporter From Influenza A. *J. Am. Chem. Soc.* **2012**, *134*, 7215−7218.
(39) Colvin, M. T.; Andreas, L. B.; Chou, J. J.; Griffin, R. G. Proton Association Constants of His 37 in the Influenza-A M218−60 Dimer-of-Dimers. *Biochemistry* **2014**, *53*, 5987−5994.
(40) Glowiak, T.; Malarski, Z.; Sobczyk, L.; Grech, E. New Example of a Symmetrical Nhn Hydrogen-Bond in Protonated 1,8 Bis-(Dimethylamino)Naphthalene (DMAN). *J. Mol. Struct.* **1992**, *270*, 441−447.
(41) Lopez, C.; Claramunt, R. M.; LlamasSaiz, A. L.; FocesFoces, C.; Elguero, J.; Sobrados, I.; AguilarParrilla, F.; Limbach, H. H. X-Ray Diffraction and Solid State NMR Studies of 1,8-Bis(dimethylamino)-naphthalene and Its Complexes with Picric and Hexafluorophosphoric Acids. *New J. Chem.* **1996**, *20*, 523−536.
(42) Parkin, A.; Wozniak, K.; Wilson, C. C. From Proton Disorder to Proton Migration: A Continuum in the Hydrogen Bond of a Proton Sponge in the Solid State. *Cryst. Growth Des.* **2007**, *7*, 1393−1398.
(43) Wozniak, K.; He, H. Y.; Klinowski, J.; Barr, T. L.; Milart, P. ESCA and Solid-State NMR Studies of Ionic Complexes of 1,8-Bis(dimethylamino)naphthalene. *J. Phys. Chem.* **1996**, *100*, 11420−11426.
(44) Crivello, J. V. Nitrations and Oxidations with Inorganic Nitrate Salts in Trifluoroacetic-Anhydride. *J. Org. Chem.* **1981**, *46*, 3056−3060.
(45) Kurasov, L. A.; Pozharskii, A. F.; Kuzmenko, V. V. Peri-Naphthylenediamines 0.3. Convenient Method for the Alkylation of 1,8-Naphthylenediamines and Perimidines. *Zhurnal Organicheskoi Khimii* **1981**, *17*, 1944−1947.
(46) Lloyd-Jones, G. C.; Harvey, J. N.; Hodgson, P.; Murray, M.; Woodward, R. L. Scalar Coupling Between the N-15 Centres in Methylated 1,8-Diaminonaphthalenes and 1,6-Diazacyclodecane: To

DOI: 10.1021/acs.jpcb.5b06171
J. Phys. Chem. B 2015, 119, 11581−11589

What Extent is (2H)J(NN) a Reliable Indicator of N-N Distance? *Chem. - Eur. J.* **2003**, *9*, 4523−4535.
(47) Ni, W. H.; Dongsheng; Shi, F.; Xue, D.; Yang, H. Hydrazine-Hydrate Catalyzed Preparation of 1,8-Dimethylaminonapthalene from 1,8-Dinitronaphthalene. CN 101823968A, 2010.
(48) Li, S.; Su, Y.; Luo, W.; Hong, M. Water-protein Interactions of an Arginine-Rich Membrane Peptide in Lipid Bilayers Investigated by Solid-State Nuclear Magnetic Resonance Spectroscopy. *J. Phys. Chem. B* **2010**, *114*, 4063−4069.
(49) Hong, M.; Gross, J. D.; Rienstra, C. M.; Griffin, R. G.; Kumashiro, K. K.; Schmidt-Rohr, K. Coupling Amplification in 2D MAS NMR and Its Application to Torsion Angle Determination in Peptides. *J. Magn. Reson.* **1997**, *129*, 85−92.
(50) Bielecki, A.; Kolbert, A. C.; Levitt, M. H. Frequency-Switched Pulse Sequences: Homonuclear Decoupling and Dilute Spin NMR in Solids. *Chem. Phys. Lett.* **1989**, *155*, 341−346.
(51) Hong, M.; Griffin, R. G. Resonance Assignment for Solid Peptides by Dipolar-Mediated 13C/15N Correlation Solid-State NMR. *J. Am. Chem. Soc.* **1998**, *120*, 7113−7114.
(52) Rienstra, C. M.; Hohwy, M.; Hong, M.; Griffin, R. G. 2D and 3D 15N-13C-13C NMR Chemical Shift Correlation Spectroscopy of Solids: Assignment of MAS Spectra of Peptides. *J. Am. Chem. Soc.* **2000**, *122*, 10979−10990.
(53) van Rossum, B.-J.; de Groot, C. P.; Ladizhansky, V.; Vega, S.; de Groot, H. J. M. A Method for Measuring Heteronuclear (H-1-C-13) Distances in High Speed MAS NMR. *J. Am. Chem. Soc.* **2000**, *122*, 3465−3472.
(54) Hong, M.; Yao, X. L.; Jakes, K.; Huster, D. Investigation of Molecular Motions by Lee-Goldburg Cross-Polarization NMR Spectroscopy. *J. Phys. Chem. B* **2002**, *106*, 7355−7364.
(55) Hoser, A. A.; Dobrzycki, L.; Gutmann, M. J.; Wozniak, K. Charge Densities of Two Polymorphs of Hydrated 1,8-Bis-(dimethylamino)naphthalene Hydrochloride-Similarities and Differences. *Cryst. Growth Des.* **2010**, *10*, 5092−5104.
(56) Pyzalska, D.; Pyzalski, R.; Borowiak, T. Structure of 1,8-Bis(Dimethylamino)Naphthalene Hydrobromide Dihydrate. *J. Crystallogr. Spectrosc. Res.* **1983**, *13*, 211−220.
(57) Wozniak, K.; Krygowski, T. M.; Kariuki, B.; Jones, W.; Grech, E. Crystallographic Studies on Sterically Affected Chemical-Species 0.2. Molecular and Crystal-Structure of 1,8-Bis(Dimethylamino)-Naphthalene Tetrafluoroborate - Analysis of Distortion of Geometry in the Aromatic Part Due to Intramolecular Hydrogen-Bonding. *J. Mol. Struct.* **1990**, *240*, 111−118.
(58) Song, X. J.; McDermott, A. E. Proton Transfer Dynamics and N-H Bond Lengthening in N-H Center dot Center dot Center dot N Model Systems: a Solid-State NMR Study. *Magn. Reson. Chem.* **2001**, *39*, S37−S43.
(59) Lopez, C.; Lorente, P.; Claramunt, R. M.; Marin, J.; Foces-Foces, C.; Llamas-Saiz, A. L.; Elguero, J.; Limbach, H. H. Localization of Hydrogen Bond Deuterons in Proton Sponges by Dipolar Solid State N-15 NMR Spectroscopy. *Berichte Der Bunsen-Gesellschaft-Physical Chemistry Chemical Physics* **1998**, *102*, 414−418.
(60) Mallinson, P. R.; Smith, G. T.; Wilson, C. C.; Grech, E.; Wozniak, K. From Weak Interactions to Covalent Bonds: A Continuum in the Complexes of 1,8-Bis(dimethylamino)naphthalene. *J. Am. Chem. Soc.* **2003**, *125*, 4259−4270.
(61) Frey, P. A.; Cleland, W. W. Are There Strong Hydrogen Bonds in Aqueous Solutions? *Bioorg. Chem.* **1998**, *26*, 175−192.

DOI: 10.1021/acs.jpcb.5b06171
J. Phys. Chem. B 2015, 119, 11581−11589

Supporting Information

^{15}N and ^{1}H Solid-State NMR Investigation of a Canonical Low-Barrier Hydrogen-Bond Compound: 1,8-bis(dimethylamino) naphthalene

Paul B. White and Mei Hong*

Department of Chemistry, Massachusetts Institute of Technology, 170 Albany Street, Cambridge, MA 02139

Full author list for reference 35:

35. Acharya, A.; Carnevale, V.; Fiorin, G.; Levine, B. G.; Polishchuk, A.; Balannick, V.; Samish, I.; Lamb, R. A.; Pinto, L. H.; DeGrado, W. F.; Klein, M. L., Structural Mechanism of Proton Transport Through the Influenza A M2 Protein. *Proc. Natl. Acad. Sci. U. S. A.* **2010,** *107*, 15075-15080.